공학석사 학위논문

2단계 소결에 의한
3Y-TZP의 미세구조 와 기계적 성질

Microstructural Evolution and Mechanical Properties of 3Y-TZP sintered by Two Step Sintering (TSS)

2014년 8월

서울대학교 대학원
재료공학부
승 현 찬

Microstructural Evolution and Mechanical Properties of 3Y-TZP sintered by Two Step Sintering (TSS)

지도교수 김현이

이 논문을 공학석사 학위논문으로 제출함

2014 년 7 월

서울대학교 대학원

재료공학부

승 현 찬

승 현 찬의 석사 학위논문을 인준함

2014년 7월

위 원 장 홍 성 현(인)

부위원장 고 영 학(인)

위 원 김 현 이(인)

Abstract

Microstructural Evolution and Mechanical Properties of 3Y-TZP sintered by Two Step Sintering (TSS)

Hyun-Chan Seung
Department of Materials Science and Engineering
Seoul National University

Bio-ceramics are being used widely as load bearing or non-load bearing implants. They are classified into bioactive and bioinert ceramics. Bioactive ceramics such as HA, TCP and biphasic materials are advantageous in terms of its injectability, low processing temperature and regeneration of tissues and bones. Bioinert ceramics such as alumina and zirconia have outstanding mechanical properties and good biocompatibility. In particular, 3Y-TZP has excellent mechanical properties compare to other bioinert implants. Many researches have been done in controlling the grain size of ceramic materials to obtain enhanced mechanical properties. In 2000, Chen and Wang designed Two Step Sintering (TSS) process which sinters ceramic at a low temperature for a very long time. Despite its low sintering temperature, below 300 °C, ceramic materials obtained small grain sizes and full densification. Many articles have reported about 3Y-TZP sintered by TSS. However, none of them mentioned about the mechanical properties of 3Y-TZP.

In this study, mechanical properties of 3Y-TZP sintered by various TSS conditions with varying 2nd-step sintering time were examined. 3Y-TZP was sintered for 15 min at 1450 °C during the 1st-step sintering to make the material fully dense, then, 2nd-step sintering temperature was set at 1150 °C and samples were sintered for 0, 6, 12, 18, 24, 30, 48, 60 and 72 hr. The measurement of relative density, grain size, microstructure, mechanical properties (flexural strength, hardness and fracture toughness) and in vitro test of the sintered body was done. All conditions of 3Y-TZP sintered by TSS process was found to reach over 99% of the theoretical density even though the relative density was observed to increase as the 2nd-step sintering time increased. Along with increasing the 2nd-step sintering time, the average grain size of 3Y-TZP was also found to increase from 153 ± 7 (0 hr sintering) to 211 ± 11 nm (72 hr sintering), which is 2 to 2.5 times as small as that of the commercial one step sintered 3Y-TZP. In particular, interesting structures, subgrains and agglomerated particles, were observed inside normal grain and some part of the surface of 3Y-TZP sintered by TSS, respectively. We predicted the grain growth mechanism in the TSS based on the results as the relationship of the 2nd-step sintering time. In this study, because all conditions were fully dense, we confirmed that grain size and subgrain effected on the mechanical properties. Flexural strength of 3Y-TZP sintered by TSS process increased up to 781 ± 45 MPa at 2nd-step sintering time, 30 hr, then considerably decreased as the 2nd-step sintering time exceeded 30 hr. Therefore, the effects of subgrain and grain size were the complete correlation,

inverse relation with flexural strength. This subgrain structure showed relation with crack propagation. 3Y-TZP sintered by TSS had cracks that penetrated inside the grain, which had subgrain, more frequently. This is the main effect on flexural strength of subgrain. However, it was believed that there exist any other factors that effected on strength besides the subgrain effect. There was not any significant difference in hardness and fracture toughness. The biological properties of 3Y-TZP also had no significant difference depending on the grain size, indicating that 3Y-TZP sintered by TSS still had very good biocompatibility without any toxicity.

Keywords: 3Y-TZP, Two Step Sintering, 2nd-step sintering time, Mechanical properties, Grain size, Subgrain.

Student number: 2012-23145

Contents

List of figures and tables

[Figure 9] Relative density depending on 2nd-step sintering time.

[Figure 10] Microstructures of 3Y-TZP from different sintering conditions: (a) one-step sintering at 1450 °C for 2 hr, (b) TSS 0, (c) TSS 6, (d) TSS 12, (e) TSS 24, and (f) TSS 72.

[Figure 11] Grain size depending on 2nd-step sintering time.

[Figure 12] Schematic diagrams of microstructures of (a) 3Y-TZP after one-step sintering at 1450 °C for 2 hr, and (b) 3Y-TZP after two-step sintering. (c) Micrograph image of 3Y-TZP through TSS 6, indicating the important features of the microstructure as compared to that through one-step sintering.

[Figure 13] High resolution images of (a) 3Y-TZP particles used in this experiment, (b) representative nanostructure of sintered 3Y-TZP through TSS 0 and (c) representative nanostructure of sintered 3Y-TZP through TSS 6. Average particle size of 3Y-TZP powders is 63 ± 5 nm, and average agglomerate particle size is 75 ± 2 nm and average subgrain size is 80 ± 5 nm from image analysis.

[Figure 14] Subgrain ratio depending on 2nd-step sintering time.

[Figure 15] Flexural strength data tested by (a) 4-point bending test and (b) biaxial bending test.

[Figure 16] (a) Hardness and (b) Fracture toughness. There is no significant difference among conditions.

[Figure 17] The morphology of crack on the 3Y-TZP sintered by TSS surface. Crack penetrated some grains, which were marked circles.

[Figure 18] Cell attachment image of (a) One-step sintered sample and (b) TSS 30. (c) Cell viability measured by an MTT assay. No statistical significance was observed between two types of 3Y-TZP for each culture time.

1. Introduction

1.1. Bio-ceramics

1.1.1. Bioactive Implant

Innumerable fractures in human bone and tooth occur around the world. Especially, large bone or various shaped defects are difficult and complicated to repair. The number of those who need surgery for bone graft has increased steadily [1]. Autografts or allografts are the approaches to settle these difficult repairs [2]. However, autograft and allograft have several disadvantages such as structural problems and immunological response, respectively [3]. Therefore, considerable studies have been looked towards hydroxyapatite (HA, $Ca_{10}(PO_4)_6(OH)_2$) and tricalcium phosphate (TCP, $Ca_3(PO_4)_2$), which dissolve in the body fluid, in other words, bioactive materials and have injectability and low temperature processing. Bioactive implant has a positive effect on the regeneration of tissues [4].

HA can bond to bone which is made in interface between bone and implant. Also, it stimulates new bone generation that is essential for stability of implant. That's why HA has been paid attention to using implant applications [5-9]. However, there is a critical limitation, its poor mechanical properties, which are much lower than those of natural bone. That makes the limit line on application of implant composed of HA. Nowadays, HA is useful only non-load-bearing implant and coating layer on the surface of metal

implants [10-12].

TCP, a kind of calcium phosphate ceramics, is bioresorbable, which means it is soluble in the body fluid. This rate of TCP is faster than HA and the parts of TCP or HA are substituted with natural tissues. For using implant to make new bone regenerated, enough strength and other mechanical performance during regeneration were required for stability of implant. However, bioactive TCP has so poor mechanical properties that it has been studied for porous body. Especially, biodegradation rate of TCP is too fast to maintain the required mechanical properties, which indicates no bone formation occur in TCP parts [13, 14].

Biphasic Calcium Phosphate (BCP) of HA and TCP were studied to confirm whether BCP is a superior biomaterials or not. In fact, it was reported to induce faster regeneration and higher mechanical properties than pure HA [15, 16], and more accelerate generation of new bone compared with pure TCP [17]. Additionally, BCP has higher bone/bone interface formation and resorption rate of it located at between with pure HA pure TCP [14].

1.1.2. Bioinert Implant

Zirconia (ZrO_2) has been widely used in bio-application because of good biocompatibility. Also, it has physical and chemical stability, high melting temperature and outstanding mechanical properties, which is used

even engineering field [18]. However, pure zirconia undergoes transformation from tetragonal phase to monoclinic phase when it is cooled down to room temperature after sintering process, resulting in highly decreased mechanical properties [19]. It has been solved by adding some additives such as Y_2O_3, MgO and CeO_2. As shown in fig 1, these additives help the zirconia to remain as tetragonal phase which is metastable phase at room temperature [20, 21]. Due to the stability of tetragonal phase of zirconia in room temperature, solid solutions such as MgO-ZrO_2, CaO-ZrO_2 and Y_2O_3-ZrO_2, were widely examined for biomedical applications [18]. If an external force is applied on the surface, tetragonal phase turn into monoclinic phase. During this phenomenon, the volume of zirconia is expanded to about ~4% and inner strain is induced in sequence. This is called transformation toughening. Also, Alumina (Al_2O_3) has been extensively used for biomaterial in terms of its excellent strength, hardness and good biocompatibility [22]. However, it has lower fracture toughness than zirconia, which is able to induce catastrophic failure. It has been already confirmed that yttria-zirconia ceramics have mechanical properties better than alumina, as shown in Table 1 [18].

1.2. Y-TZP

Researchers have paid attention to yttria-tetragonal zirconia polycrystals (Y-TZP). Y-TZP has higher fracture toughness than other

zirconia based ceramics and has good biocompatibility for using implant, as shown in Table 2 [23-25]. Those excellent properties of Y-TZP depend on the microstructures and phases. These are determined by amount of Y_2O_3 in Y-TZP. There have been many researches on grain-boundary characterization to find the correlation between amount of additives, Y_2O_3, and phase. To analyze grain growth, for example, Lange, Sakuma and Yoshizawa used dual-phase structure which consisted of tetragonal and cubic grains. They found that Y-TZP (2, 3 mol %)'s grain growth rate is slower than that of Y-CSZ (8 mol %). And Matsui et al. studied the microstructures of 2, 3 and 8 mol % Y_2O_3-containing zirconia to propose the grain growth mechanism. They explained the difference of Y-TZPs and Y-CSZ using Y^{3+} ion segregations. The segregations depended on sintering time and amount of Y_2O_3, which induced distinction of phase fraction in the materials. Fig 2 shows the dependence of the fractions of cubic, tetragonal and monoclinic phases in 2, 3 and 8 mol % Y_2O_3 [26].

In particular, 3 mol % Y_2O_3, 3Y-TZP, had lower monoclinic phase and the highest fraction of tetragonal phase. According to Chevalier and Gremillard et al. [21] and Chevalier et al. [27], monoclinic phase induces lower mechanical properties and cubic phase has critical effect on low temperature degradation [28]. That's why 3Y-TZP was more widely used in many fields than other Y-TZPs.

1.3. Sintering

1.3.1. Sintering mechanism

Sintering is one of the most important and the oldest synthesis and processing [29]. It is a heat treatment for bonding particles via atom and grain boundary diffusion to reduce surface free energy. Men have ultimately sought ‘microstructural control’ through sintering, which involves controlling the grain size, density and the distribution and size of pores during the fabrication process [30]. Fig 3(a) represents conventional sintering process, which is clarified with three stages. In detail, at initial stage, necking between adjacent particles forms with fast densification and slow coarsening. Coarsening induces grain growth and densification packs the powders resulting higher density (Fig 3(b)). As temperature goes up, densification rate becomes lower and grain growth rate becomes higher. Finally, the final stage has the most active coarsening, which causes dramatic grain growth (Table 3) [29]. However, although we pursue an ultra-fine grained microstructure which is related to better mechanical properties to the ceramics, sintered ceramics through the conventional process must be made to coarse grain size (Fig 4). There are several ways to reduce grain size by adjusting variables. But, controlling one variable induces another bad effect. For examples, decreasing in particle size causes greater expense and higher impurity level and decreasing in sintering time leads to lower density. Therefore, many researchers have studied other processes, which are different from existing

sintering process.

1.3.2. Two Step Sintering (TSS)

It has been reported that toughed ceramics have higher hardness and superplastic deformation as they have an ultrafine grain [31]. Hence, many processes have been studied to get smaller grain, nano-scale grain size of sintered ceramics. It was first succeeded to make the materials with fully dense nano-grained in 2000 by Chen and Wang, who made a change in the conventional sintering process. They restrained grain growth by extending intermediate stage without the final stage (Fig 5(a)). It is called Two Step Sintering (TSS). This was available because there is the difference in kinetics between grain-boundary diffusion and grain-boundary migration at the sintering temperature of the intermediate stage, which suppressed the final-stage grain growth [32]. There are the core conditions in TSS. (1) Heating T_1, 1^{st}-step sintering temperature, to achieve certain critical density to make pores unstable. (2) Decreasing T_2, 2^{nd}-step sintering temperature, to sinter the specimens without grain growth [31]. This process has been widely used to restrain grain growth in sintering process for other ceramics, ZnO [33], $BaTiO_3$ [34] and Al_2O_3 [35].

In case of Y-TZP, Mazaheri et al. obtained 3Y-TZP which was fully dense with an average grain size of 100 nm by sintering at 1150 ^oC for 30 hr

for the 2nd-step (Fig 5(b)) [32]. Lourenco et al. obtained dense low yttria-containing zirconia with the average grain size of ~100 nm, which was indicating the threshold of the nano-scale [36]. Moerover various fabrication methods were applied to TSS for nano-sized grain of Y-TZP. Yu et al. studied TSS of nano-sized Y-TZP process using powder injection moulding [37]. Reddy et al. analyzed TSS, even multi-step process, using spark plasma sintering [38, 39]. Interestingly, Maca et al. asserted the opposite result that tetragonal phase zirconia based ceramics were not affected by TSS on restraint grain growth (Fig 5(c) [40], Table 4 [31, 36, 39-41]).

1.4. Aim of this study

Mechanical properties of ceramic materials depend on several factors, microstructure, grain size, density (porosity), and second-phase particles and so on. However, lots of articles analyzing the mechanical properties of 3Y-TZP via one step sintering didn't consider the relative density to explain the correlation between grain size and some mechanical properties even though ceramic materials with smaller grain size cannot have bending strength enough to be used in applications [23, 25, 28]. Also, there was not any reported improvement on mechanical properties of the ceramic that is processed by TSS. Therefore, in this study, to control the effect from the difference of relative density, 3Y-TZP was sintered at higher 1st-step sintering

temperature, 1450 ^{o}C, than published articles, below 1350 ^{o}C, to make all samples fully dense and we analyzed mechanical properties of 3Y-TZP fabricated by TSS through several sintering conditions. Hence, we clarified the correlation between grain size and density with the second-step sintering time and also examined which variable was the most influential on the mechanical properties of 3Y-TZP.

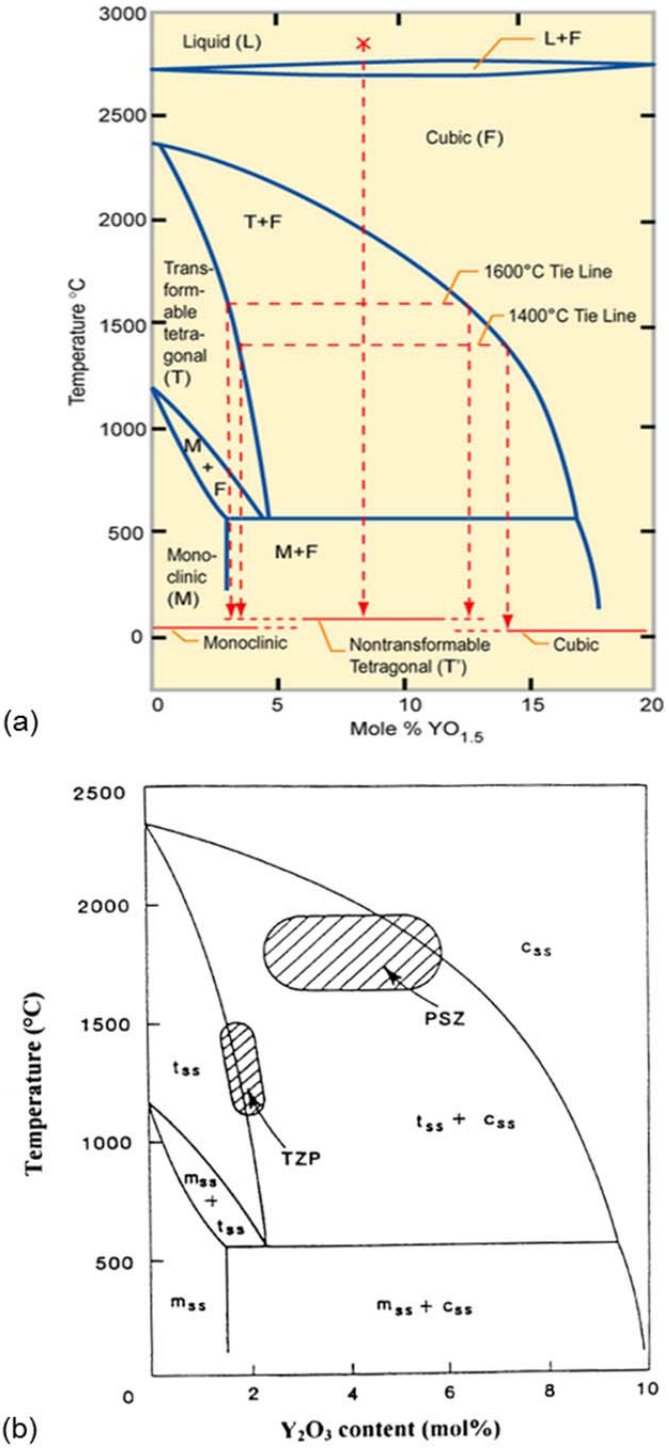

[Figure 1] Phase diagram of yttria-containing zirconia (Y-TZP) [18].

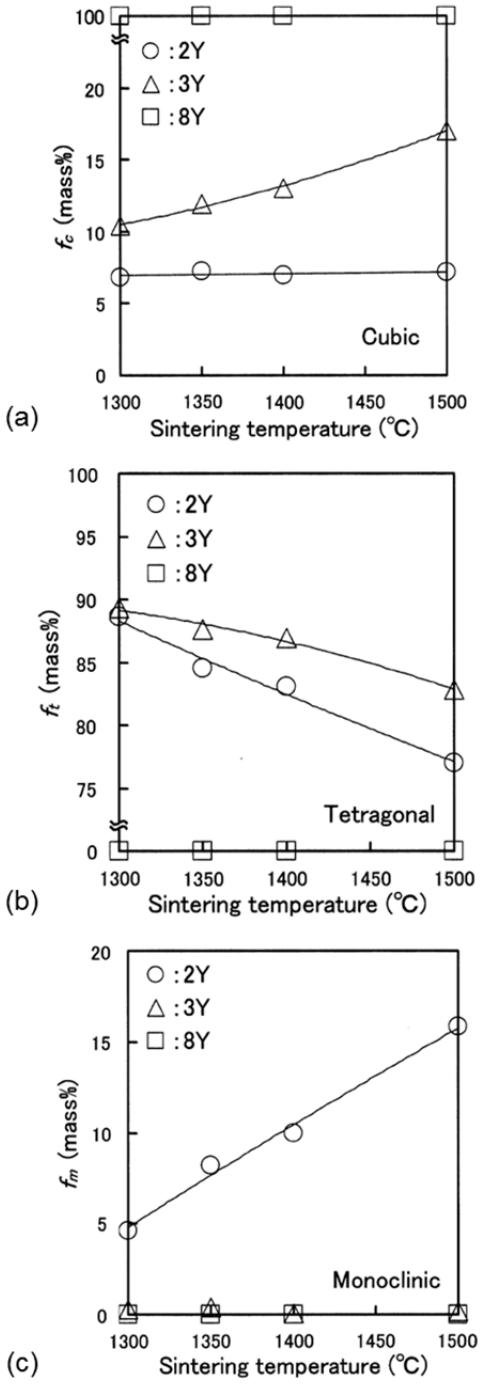

[Figure 2] Dependence of the fractions of cubic, tetragonal and monoclinic phases in 2Y, 3Y and 8Y with sintering temperature [26].

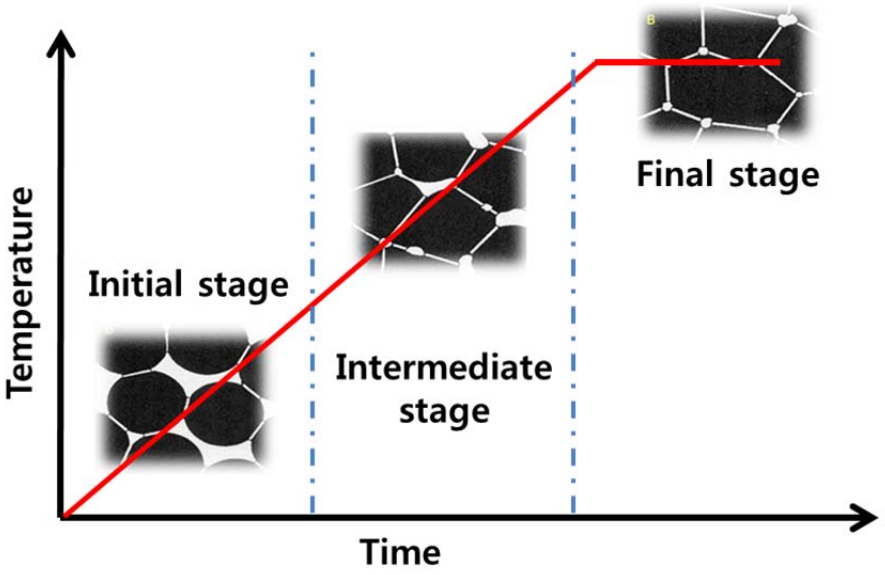

(a)

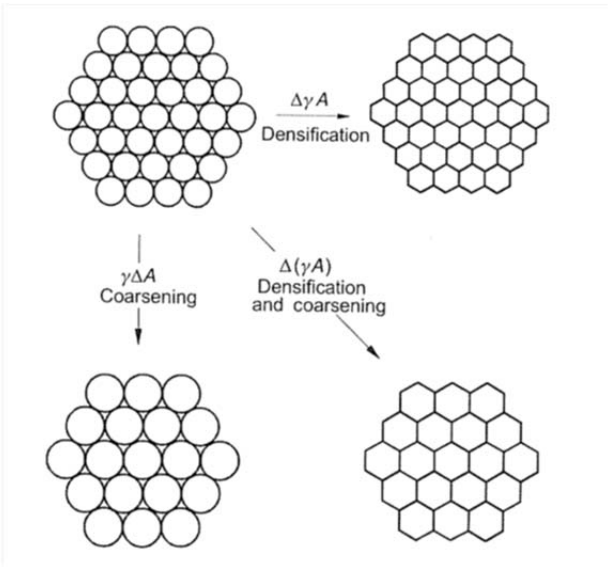

(b)

[Figure 3] The schematic diagram of conventional sintering process (a) and densification and coarsening (b)[29, 30].

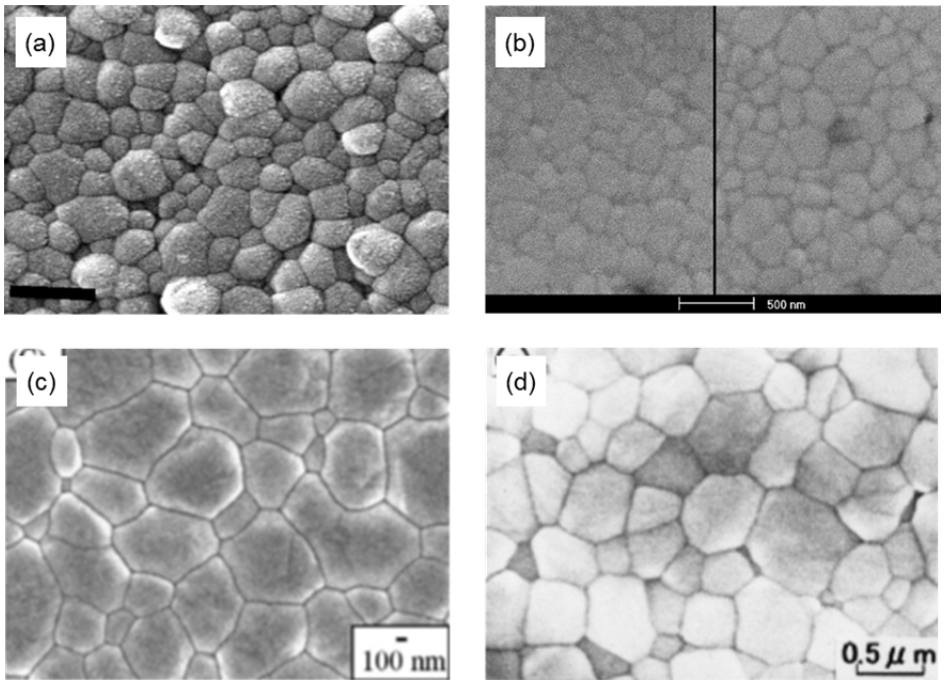

[Figure 4] The microstructure image of 3Y-TZP sintered by several sintering condition, (a) 1250 ^{o}C for 12 hr after 1300 ^{o}C for 1 min [31], (b) left; 1275 ^{o}C for 10 hr after 1305 ^{o}C and right; 1405 ^{o}C for 0 min [40], (c) 1600 ^{o}C for 2 hr [42], (d) 1350 ^{o}C for 5 hr [43].

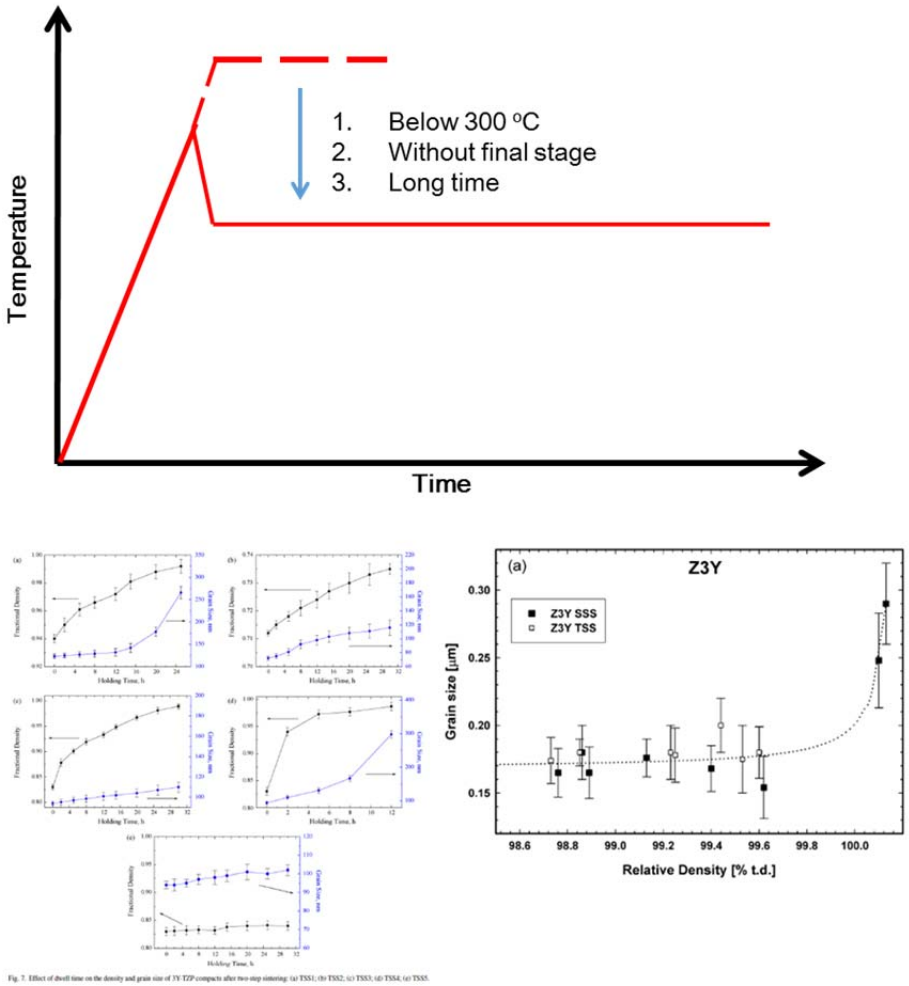

[Figure 5] (a) The schematic diagram of two step sintering process (b) and (c) Relative density vs. grain size of 3Y-TZP sintered by TSS [31, 40].

Property	Units	Alumina	Mg-PSZ	TZP
Chemical composition		99.9% Al_2O_3 + MgO	ZrO_2 + 8~10 mol% MgO	ZrO_2 + 3 mol% Y_2O_3
Density	g cm^{-3}	≥ 3.97	5.74-6	> 6
Porosity	%	< 0.1	-	< 0.1
Bending strength	MPa	> 500	450-700	900-1200
Compression strength	MPa	4100	2000	2000
Young modulus	GPa	380	200	120
Fracture toughness, K_{IC}	MPa m^{-1}	4	7-15	7-10
Thermal expansion coefficient	K^{-1}	8×10^{-6}	$7\text{-}10 \times 10^{-6}$	11×10^{-6}
Thermal conductivity	WmK^{-1}	30	2	2
Hardness	HV 0.1	2200	1200	1200

[Table 1] Characteristics of some ceramics for biomedical application [18].

Material	Strength (MPa)	Fracture Toughness (MPa $m^{1/2}$)	Elastic Modulus (GPa)	Hardness (GPa)
E1	106 (17)	1.2 (0.14)	65 (1.5)	6.5 (0.4)
E2	303 (49)	3.0 (0.65)	90 (3.7)	5.5 (0.2)
EC	306 (29)	2.9 (0.51)	105 (4.8)	5.3 (0.2)
IA dry-pressed	440 (50)	3.6 (0.26)	265 (10)	11 (1.1)
IZ dry-pressed	476 (50)	4.9 (0.36)	240 (9.0)	11 (0.9)
IA slip	594 (52)	4.4 (0.48)	265 (10)	11 (0.3)
IZ slip	630 (58)	4.8 (0.50)	240 (9.0)	10.5 (0.2)
YZ	680 (130)	5.5 (0.34)	240 (9.5)	13 (0.3)
DZ	840 (140)	7.4 (0.62)	220 (7.5)	12 (0.2)

[Table 2] Averages of flexural strength and fracture toughness of all materials [24, 25].

Stage	Process	Surface Area Loss	Densification	Coarsening
Adhesion	Contact formation	Minimal unless compacted at high pressures	None	None
Initial	Neck growth	Significant, up to 50% loss	Small at first	Minimal
Intermediate	Pore rounding and elongation	Near total loss of open porosity	Significant	Increase in grain size and pore size
Final	Pore closure, final densification	Negligible further loss	Slow and relatively minimal	Extensive grain and pore growth

[Table 3] Classic stages of sintering [29].

T_1 (°C)	Cooling rate (K min^{-1})	T_2 (°C)	T_2 (h)	Grain size (nm)	Ref.
1305	60	1275	10	180	[31]
1300	Natural cooling	1200	15	125	[36]
1300	50	1150	30	110	[39]
1305	60	1275	10	170	[40]
1300	20	1270	12	113	[41]

[Table 4] Literature review of two-step sintering of 3Y-TZP ceramics with relative density higher than 93%.

2. Material and methods

2.1. Material

ZrO_2-3 mol% Y_2O_3 (3Y-TZP) powder consists of ZrO_2 and Y_2O_3 at a molar ratio of 97:3. 3Y-TZP powder, which is a primary particle with an average size of approximately 60 nm, was supplied from Tosoh Co. (Tokyo, Japan).

2.2. Sintering process of ceramic green bodies

The powders were compacted in a cylindrical die under the pressure of 50 MPa to produce green compacts with a diameter of 60 mm and a height of 13 mm. The green body, of which density was ~48% of the theoretical density, was densified under a hydrostatic pressure of 200 MPa for 5 min using Cold Isotactic Pressure (CIP) equipment. Before the sintering, all of the compacts were pre-sintered at 1000 ^{o}C to make the dimension of 4 mm × 5 mm × 40 mm (Fig 6(a)), for several measurements except for the biaxial bending test; it require disk-shaped sample, which was made with a diameter of 16.5 mm and a height of 1.8 mm without pre-sintering. The pre-sintered body was sintered under various sintering conditions using the SIC box furnace (AJ-SB3, Ajeon Heating Industrial Co., Korea) with the heating and cooling rate of 5 ℃min^{-1} and 20 ℃min^{-1} respectively [36]. Various sintering conditions are shown in Table 5. 1st-step sintering temperature was 1450 ℃, which is higher than the sintering temperatures that were reported, in order to make fully densified sample. For the 2nd-step sintering, the compacts were cooled down to 1150 ℃, which was shown as results of the fully dense and smallest grain

size of 3Y-TZP via TSS in among the articles (Table 4), and maintained for 0, 6, 12, 18, 24, 30, 48, 60 and 72 hr in air furnace (Table 5). Then, they were cleaned at sonication for 30 min in ethanol.

2.3. Characterization

2.3.1. Phase analysis

The existence of the monoclinic phase of all the samples and powder were determined by using X-ray diffraction (XRD). The patterns were taken by Cu Kα radiation (D8-Advance, Bruker Miller Co., Germany) from 20 to 70 (2θ) at a scan rate of 1 ˚/min.

$$X_m = \frac{I(11\bar{1})_m + I(111)_m}{I(11\bar{1})_m + I(111)_m + I(111)_t} \times 100\ (\%)$$

, where $I(11\bar{1})_m, I(111)_m$ and $I(111)_t$ are the intensity of $(11\bar{1})$ and (111), which is monoclinic phase, and (111), tetragonal phase, respectively [44].

2.3.2. Density of ceramic bodies

The final relative densities of the sintered samples were measured by water displacement (Archimedes) method according to ISO Standard 39231/1-1979(E);

$$\rho_{examined} = \frac{w_1}{w_2 - w_3}\ (g/cm^3)$$

$$\rho_{relative} = \frac{\rho_{examined}}{\rho_{theoretical}} \times 100\ (\%)$$

, where ρ is the density, w_1 is the dry weight, w_2 is hydrous weight and w_3 is the underwater weight. $\rho_{theoretical}$ indicates the general density of 3Y-TZP, 6.08 g/cm^3. To estimate the density, three kinds of weight (underwater, hydrous and dry) were measured in sequences. The specimens were immersed in distilled water which was boiled for about 3 hr to fill up pores. Then, they were cooled down at room temperature to take underwater weight. After that, all droplets on surfaces were removed before weighing hydrous mass. To weigh the samples in dry condition, they were dried at 150 ℃ for 3 hr and cooled at room temperature. The sample's measured weights were calculated by taking three kinds of mass 7 times each and averaging each of them.

2.3.3. Microstructure of sintered specimens

To calculate the average grain size, the sintered bodies were mechanically polished up to diamond slurries with 1 μm (ALPHA TRADING CO.) using grounding machine (HRG-150, Daesan Machinery Ind. CO., Korea) and polishing machine (MODEL AL-12, Alpha Seiko, Japan) and thermally etched at 200 ℃ below the 2nd-step sintering temperature, 950 ^{o}C, to expose the grain boundaries. The grain size was determined by linear intercept method (ASTM Standard E112) [45]. The microstructure of the sintered 3Y-TZP was observed by Field-Emission Scanning Electron Microscope (SUPRA 55VP, Carl Zeiss, Germany). Three samples were examined for each condition and five microstructure images were analyzed for each sample; twenty line segments were used to determine the grain

size for each microphotograph.

The subgrain ratio (ω), which is the percent of grains that have subgrain inside and agglomerated particles, was calculated to check the microstructure behavior.

$$\omega = \frac{The\ grains\ that\ have\ subgrain\ and\ agglomerated\ particles}{All\ of\ the\ grains} \times 100\ (\%)$$

2.3.4. Flexural Strength of ceramic bodies

The same polishing procedure mentioned above was performed to treat the surface of the $3\,\mathrm{mm} \times 4\,\mathrm{mm} \times 40\,\mathrm{mm}$ samples before testing its flexural strength. The screw driven load frame (Instron 5582, Instron Corp., Canton, MA, USA) was used to examine flexural strength by the 4 point bending test at a constant crosshead speed of 1 $\mathrm{mm/min}$ (Fig 6(b)). The flexural strength was calculated by the following formula.

$$\sigma = \frac{3PL}{4wb^2}\ (MPa)$$

, where P is the maximum applied load (N), L is distance between support rollers (mm), w is a width of the sample (mm) and b is a height of the sample (mm).

For biaxial bending test, sintered samples were polished by the same procedure. Also, the machine was used at a constant crosshead speed of 1 mm/min (Fig 6(c)). The flexural strength was calculated by the following formula.

$$\sigma = -0.2387\mathrm{P}(\mathrm{X} - \mathrm{Y})/b^2$$

, where P is the maximum applied load (N), b is a thickness of the sample (mm).

$$X = (1 + v) \ln\left(\frac{r_2}{r_3}\right)^2 + [\frac{1 - v}{2}](\frac{r_2}{r_3})^2$$

$$Y = (1 + v)\left[1 + \ln\left(\frac{r_1}{r_3}\right)^2\right] + (1 - v)(\frac{r_1}{r_3})^2$$

, where v is the Poisson ratio, r_1 is a radius of the ball that supported the sample (mm), r_2 is a radius of the ball that pressed the sample (mm) and r_3 is a radius of the sample (mm).

2.3.5. Hardness and Fracture toughness

Hardness and fracture toughness were measured using the indentation method with an applied load of 98 N (10 kgf). The indentation time was 10 sec according to the Vickers hardness tester (HV-114, Mitutoyo, Japan) manual. The Vickers hardness was calculated by the following formula.

$$H_v = \frac{1.854 \times 9.807 \times F}{D^2} \ (MPa)$$

, where F is applied load (kgf) and D is arithmetic mean distance of the two diagonals (mm). Fracture toughness was calculated by the formula (Fig 7 [46]).

$$K_{IC} = \frac{9.052 \times 10^{-3} \times H^{3/5} E^{2/5} d}{c^{1/2}} \ (MPa\ m^{\frac{1}{2}})$$

, where H is the calculated hardness (MPa), E is the young's modulus of the sample (MPa), d is arithmetic mean distance of the two diagonals (mm) and c is the average length of the four Pamqvist cracks. 10 samples were tested to obtain the average and standard deviation.

2.4. *In vitro* biological analysis

Two kinds of samples, the conventional one which was sintered at 1450 ^{o}C for 2 hr and TSS 30) with a diameter of 16.5 mm were prepared to investigate cellular response by using MC3T3-E1 cells (ATCC, CRL-2593; Rockville, MD). Cells were seeded on each sample at a density of $3x10^4$ cells/ml and cultured in a Minimum Essential Medium (α-MEM, Welgene Co, Ltd., Korea) including 10% Fetal Bovine Serum (FBS, Life Technologies, Inc., USA) and 1% antibiotics (100 U/ml penicillin and 100 μg/ml streptomycin, GIBCO, Grand Island, NY) in a humidified incubator with 5% CO_2 at 37 °C. Initial cell attachment after 1 day and cell proliferation after 3 days and 7 days were evaluated. Before the morphology of cells on the samples were observed by scanning electron microscopy, the cells were fixed with 2.5% glutaraldehyde for 10 min followed by dehydration in graded ethanol (70, 95, and 100%). The samples were immersed in hexamethyldisilazane for 10 min then air dried. MTS assay (CellTiter 96 Aqueous One Solution, Promega, USA) was performed to measure cell viability.

2.5. Statistical analysis

The data are presented as the mean ±SE of mean. Statistical analysis was performed using a one-way analysis of variance (ANOVA) and p values less than 0.05 were considered to be statistically significant.

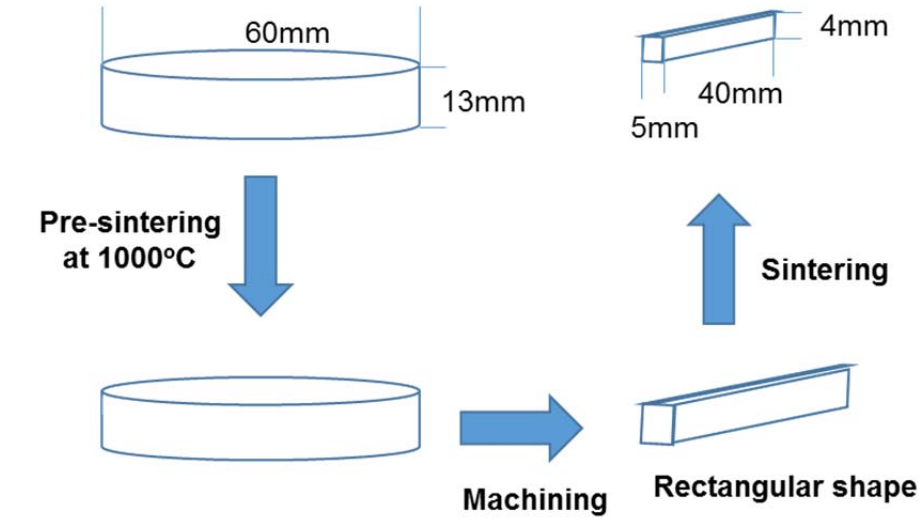

(a)

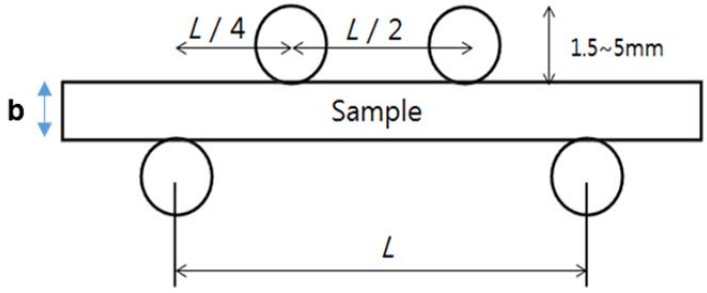

(b)

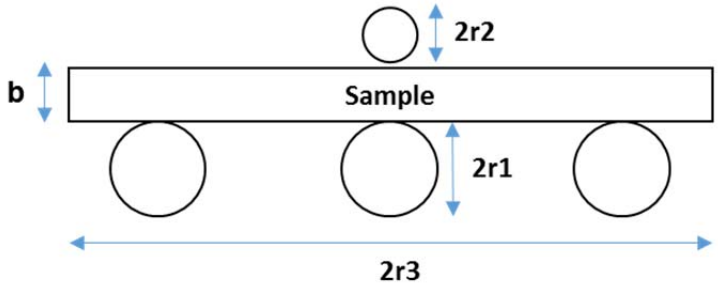

(c)

[Figure 6] (a) Processing procedure for fitting samples to measure several characteristic. The schematic diagram of 4-point bending test (b) and biaxial bending test (c).

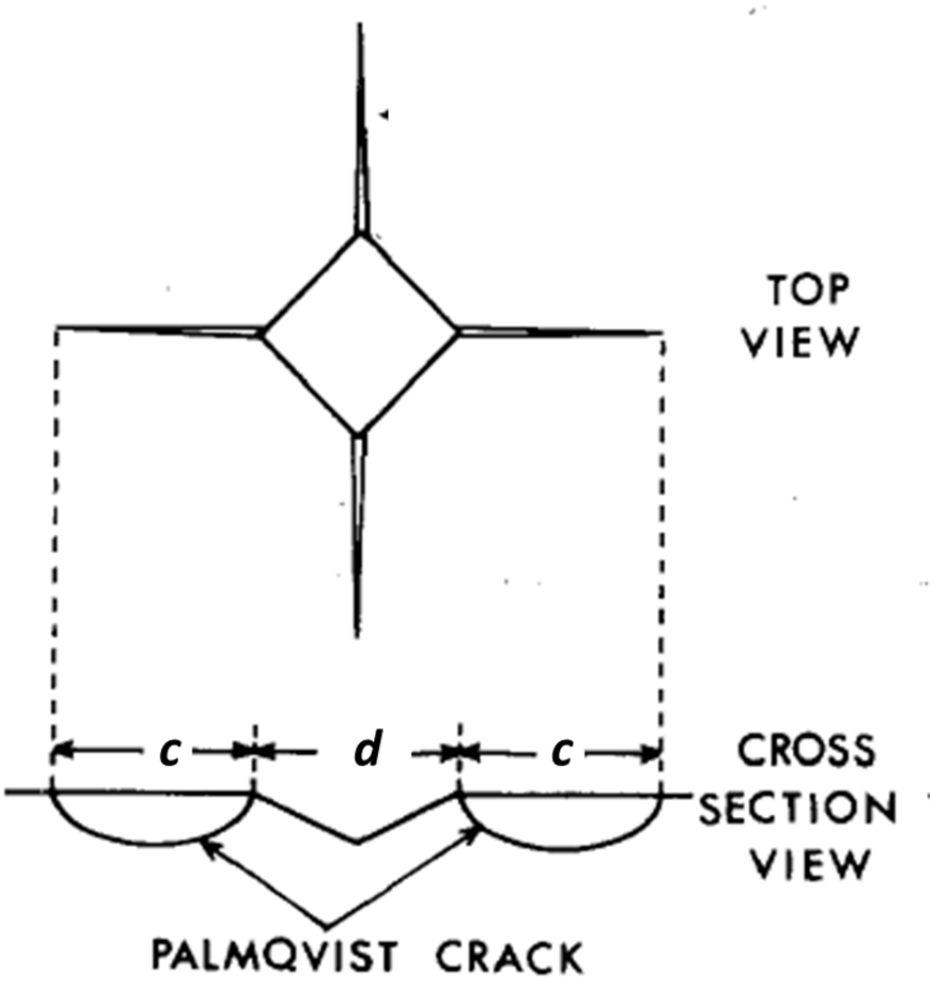

[Figure 7] The schematic diagram of micro-indentation's trace. d is diagonal of indentation and c is length of crack [46].

	1st-step		2nd-step	
	T (°C)	t (min)	T (°C)	T (hr)
TSS 0	1450	15	1150	0
TSS 6				6
TSS 12				12
TSS 18				18
TSS 24				24
TSS 30				30
TSS 48				48
TSS 60				60
TSS 72				72

[Table 5] Various Two Step Sintering conditions.

3. Results and discussion

3.1 Phase analysis and relative density of 3Y-TZP

The 3Y-TZP powder consisted of about 21 wt. % monoclinic phase and 79 wt. % tetragonal phase (Fig 8(a)). However, after TSS, monoclinic phase disappeared on X-ray diffraction pattern (Fig 8(c)), indicating no significant difference from one step sintering (Fig 8(b)). Therefore, it was confirmed that 3Y-TZP still had transformation toughening, which was the main strengthening mechanism to enhance mechanical properties of 3Y-TZP.

Through one-step sintering, the relative density reached 99.5 $\pm$ 0.2 %. However, the initial relative density through TSS started from 99.1 $\pm$ 0.2 %, which is significantly lower than that through one-step sintering ($p < 0.05$). On the other hand, the sintering time of the 2nd-step was longer, the values of relative density steadily increased from 99.1 ± 0.2 % to 99.8 ± 0.1 %, which is significantly higher than that through one-step sintering. Even though the level of densification shows significant variation depending on a sintering method and sintering time, all samples were found to reach more than 99% relative density, indicating that they could be regarded as fully dense specimen. Therefore, it was negligible to consider the difference of density when several sintering conditions of 3Y-TZP sintered through TSS were compared to each other about flexural strength.

3.2. Microstructure in the TSS system

The microstructures of 3Y-TZP obtained from different sintering methods were shown in Fig. 10. One-step sintering at 1450°C for 2h exhibits a well-developed grain structure (Fig. 10a), which is often observed in previous studies [31, 40, 42, 43]. On the other hand, two-step sintering at 1150°C led to unprecedented microstructures where various grains or agglomerate particles were mixed heterogeneously regardless of sintering times (Fig. 10b-f). In particular, subgrains and agglomerated particles were observed within a grain. Even though the sintering time of the second step increased up to 72 hr, the unique features found in the microstructures of 3Y-TZP still remained almost the same except for grain growth and relative portion of patterns.

The observed grain size of each 3Y-TZP specimen was measured through the line-intersection method. Before measuring the grain size, microstructural images of 3Y-TZP samples from the TSS methods were analyzed in order to distinguish between grains with and without subgrains. Also, regions with agglomerate particles were excluded in order to see the effect of 2^{nd}-step sintering times on grain growth. One-step sintering at 1450°C for 2h was found to grow grains with the size of ~420 nm. On the other hand, TSS methods exhibit significantly smaller grains than one-step sintering. Under all TSS conditions, grain sizes of the densified 3Y-TZP approximately ranged from 153 ± 7 to 211 ± 10 nm, which were 2 to 2.5 times as small as those of the conventional one, about 420 nm (Fig 11). Regarding the 2^{nd}-step sintering time, grain size was likely to increase along with increased sintering

time. In particular, comparing to the grains from TSS 0, grains from TSS 72 shows significant grain growth by ~40%.

The schematics of featured microstructures observed from various microstructure images (Fig. 10) were proposed in Fig. 12. Fig. 12a shows the microstructure of 3Y-TZP from one-step sintering where grains were well developed through the sintering process. The featured microstructure of 3Y-TZP through various TSS methods indicates two important features: (1) subgrains within grains and (2) agglomerated particle regions without any clear grain boundaries. A micrograph image of 3Y-TZP obtained from TSS 12 in Fig. 12(c) clearly shows those two features. To understand the origin of those features, the size of 3Y-TZP powers was measured through SEM images in Fig. 13(a). The particle size was found to range from 60 to 70 nm. After the first step sintering of the TSS method (TSS 0 and 24), the agglomerate particle regions and subgrains were observed clearly (Fig. 13(b) and 13(c)), where the sizes of particles or subgrains were found to be comparable to that of 3Y-TZP powers. Even though particles in agglomerated particle regions or subgrains within grains are larger than 3Y-TZP powers by the diameter of ~ 10 nm, the similarity in size as well as shape of particles among them indicates that those features are the metastable phase of 3Y-TZP grains before the grains are fully formed. We predicted the grain growth mechanism in the TSS based on the results as the function of the 2^{nd}-step sintering time. Grain growth occurred heterogeneously, mainly on final stage [30], which almost doesn't exist on TSS; In TSS, however, very small grains, subgrains and agglomerated

particles, appeared, as shown in Fig. 11. Fig. 14 showed the decreasing tendency of subgrain ratio of the sample sintered by TSS, 91 ± 0.03 %, 88 ± 0.01 %, 85.9 ± 0.03 %, 84 ± 0.03 % and 81 ± 0.01 % as increasing the 2^{nd} –step sintering time. Commonly, during sintering process, powders agglomerate each other and then turn into subgrains and finally they become grains. But, at 1150 ^{o}C, supplied energy was too insufficient for grain growth over whole specimen. Grain-boundary diffusion, which induced grain growth, was suppressed and only grain-boundary migration occurred by about 300 ^{o}C lower temperature than conventional sintering system. This kinetic energy was remained as long as period in 2^{nd}-step so that caused the lower subgrain ratio.

3.3. Mechanical Properties in the TSS system

Fracture strengths of 3Y-TZP by TSS had good agreement with the overall tendency of relative density, which slightly increased along with 2^{nd}-step sintering time, until 30 hr where 3Y-TZP had the maximum flexural strength (Fig 15). In particular, In case of the samples which were sintered for 30 hr, the strength was taken higher value than that of conventionally sintered one. After 30 hr, flexural strength showed a downward with increasing grain size. Generally, grain size is said to have the inverse relation with fracture strength because the possibility of creating defects is decreasing as grain size become smaller. However, the strength of 3Y-TZP is become lower although 3Y-TZP has smaller grain size up to 30 hr for 2^{nd}-step sintering time in this

study (Fig 11 and 15). According to the two graphs, two phenomena can be confirmed; (1) before 30 hr in 2^{nd}-step sintering, the strength is increased with dwindling the ratio despite of increased grain size. (2) After that, although subgrain ratio had a constant value, the strength decreased. Therefore, two interesting points were inferred according to those facts; (1) when the ratio reaches a certain point it had a stronger effect on strength compare to grain sizes (2) the existence of other factors that affect the strength of 3Y-TZP was confirmed by looking at the strength behavior after 30 hr. A significant difference in strength between TSS 30, 48 (and 60) and 72 was observed despite the 20 nm difference in grain sizes. Therefore, we discovered that apparent grain size was not the only important factors that had an effect on the strength of 3Y-TZP.

We assumed that subgrain has different microstructure with general grain boundary, which could be considered malfunctioned grain boundary. Subgrains within the normal grains were less stable than the other grains because of incoherent subgrain boundary between them [48]. Meanwhile, it was reported that cracks propagated within grain and also grain-boundary in the fully dense 3Y-TZP [25]. However, 3Y-TZP sintered by TSS had cracks that penetrated some grains like non-fully dense material with more frequency (Fig 16). In this case, it could be considered that subgrains induced unstable within grain and then cracks propagated more easily inside the grain that consisted of subgrains. That's why the strength showed higher value along with decreasing the ratio.

Hardness and fracture toughness respectively had very similar number each condition unlike flexural strength (Fig 17). It was reported that Grain size ranging from 100 to 400 nm didn't have any effect on fracture toughness of 3Y-TZP [47]. When zirconia becomes fully dense, it is found that there wasn't significant difference in hardness and fracture toughness among zirconia samples with grain sizes of 100 ~ 400 nm. 3Y-TZP that was sintered by one step or two step sintering exhibit a hardness of 12500 to 13000 MPa and a fracture toughness of 4.5 ($MPa*m^{1/2}$), approximately

3.4. *In vitro* biological analysis

Biocompatibility of 3Y-TZP prepared by different sintering methods was evaluated in order to confirm whether the TSS method significantly influences on biological performance of 3Y-TZP as compared to that from one-step sintering. Fig. 18(a) and (b) showed cell attachment on the surfaces of 3Y-TZP sintered by one step sintering and TSS 30, respectively. Cell proliferation of them appeared to be almost identical, showing no significant difference between them as shown in Fig. 18(c). The level of cell proliferation consistently increases for two types of 3Y-TZP as the culturing time are longer, indicating that both 3Y-TZP samples are non-toxic and biocompatible. It is likely to show that heat treatment methods don't influence on biocompatibility of 3Y-TZP, and instead the composition of 3Y-TZP is a key factor to determine biocompatibility from this experiment.

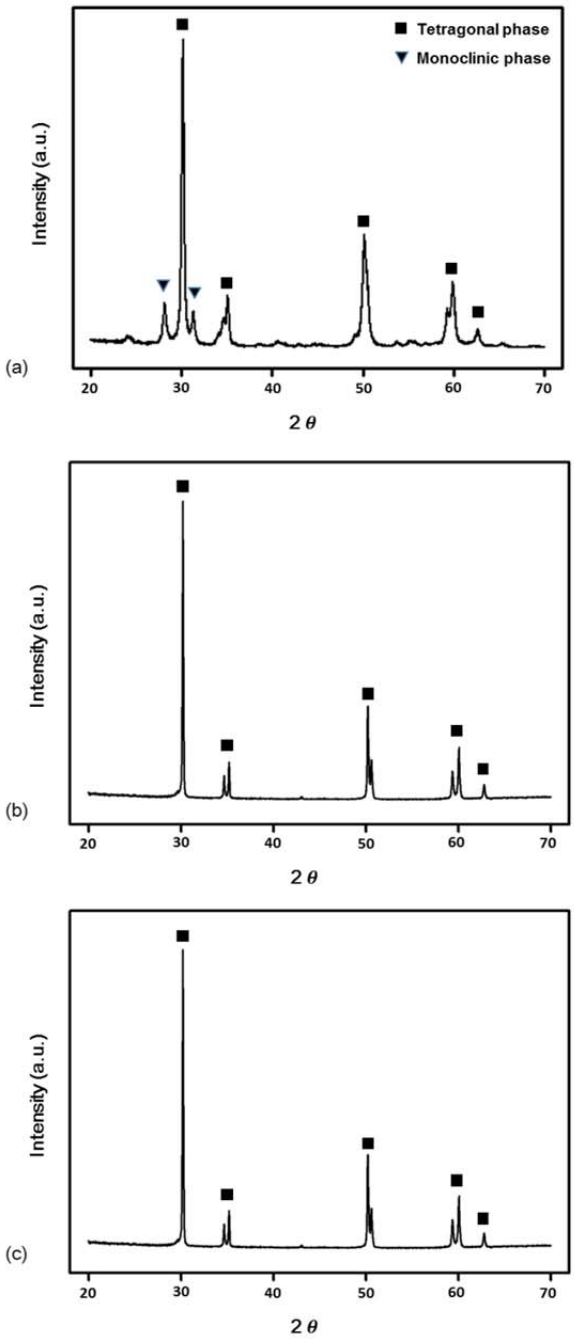

[Figure 8] XRD pattern of 3Y-TZP powder (a), one step sintering (b) and TSS 30 (c).

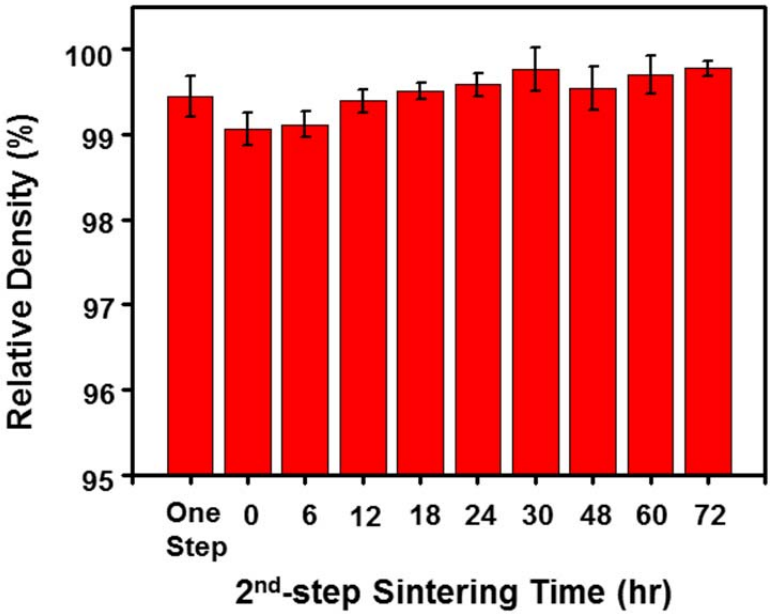

[Figure 9] Relative density depending on 2nd-step sintering time.

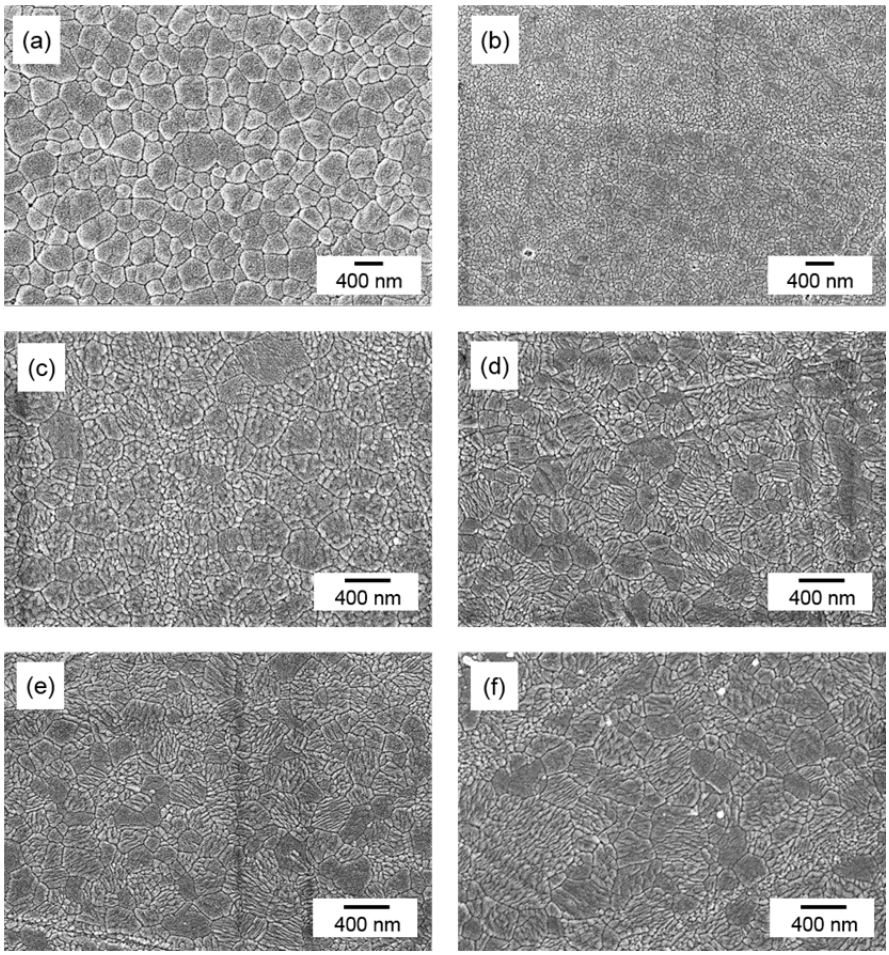

[Figure 10] Microstructures of 3Y-TZP from different sintering conditions: (a) one-step sintering at 1450 °C for 2 hr, (b) TSS 0, (c) TSS 6, (d) TSS 12, (e) TSS 24, and (f) TSS 72.

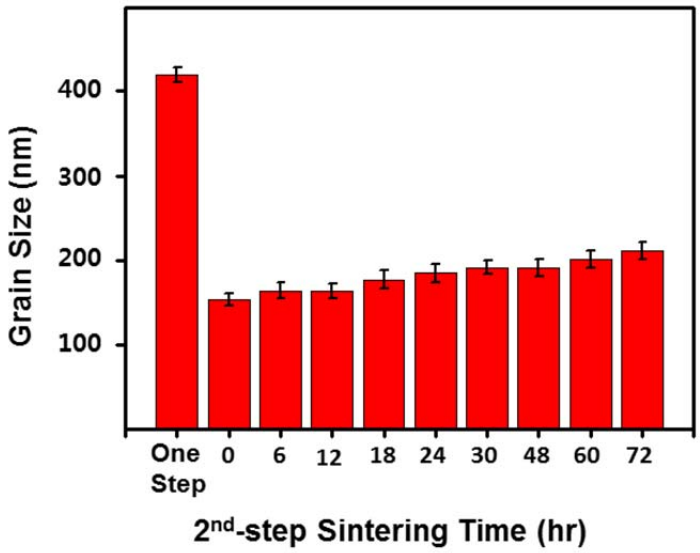

[Figure 11] Grain size depending on 2nd-step sintering time.

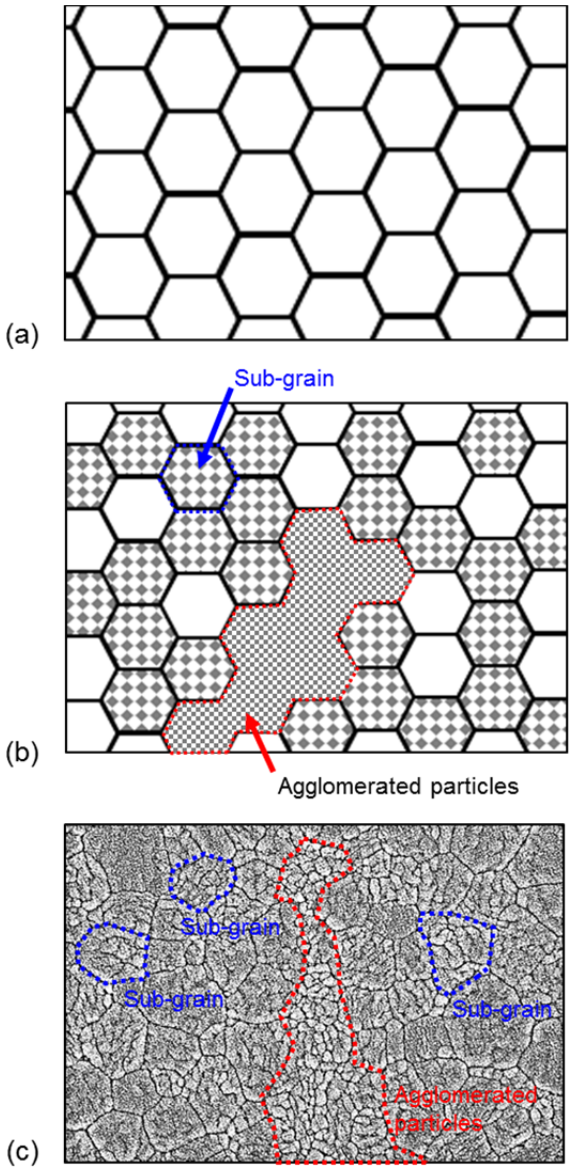

[Figure 12] Schematic diagrams of microstructures of (a) 3Y-TZP after one-step sintering at 1450 °C for 2 hr, and (b) 3Y-TZP after two-step sintering. (c) Micrograph image of 3Y-TZP through TSS 6, indicating the important features of the microstructure as compared to that through one-step sintering.

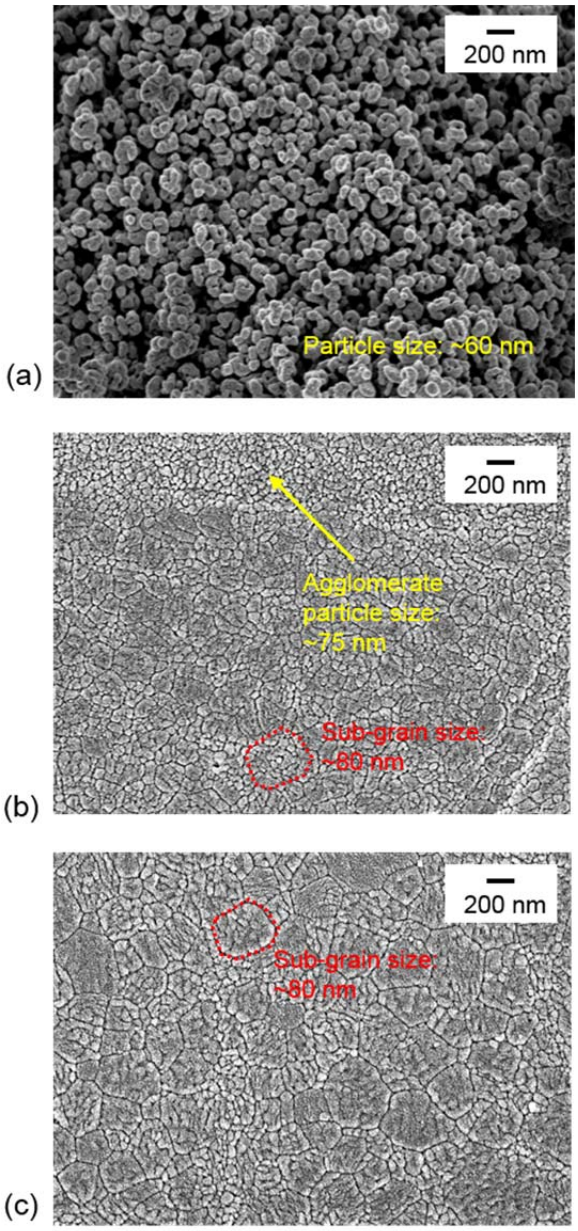

[Figure 13] High resolution images of (a) 3Y-TZP particles used in this experiment, (b) representative nanostructure of sintered 3Y-TZP through TSS 0 and (c) representative nanostructure of sintered 3Y-TZP through TSS 6. Average particle size of 3Y-TZP powders is 63 $\pm$ 5 nm, and average agglomerate particle size is 75 $\pm$ 2 nm and average subgrain size is 80 $\pm$ 5 nm from image analysis.

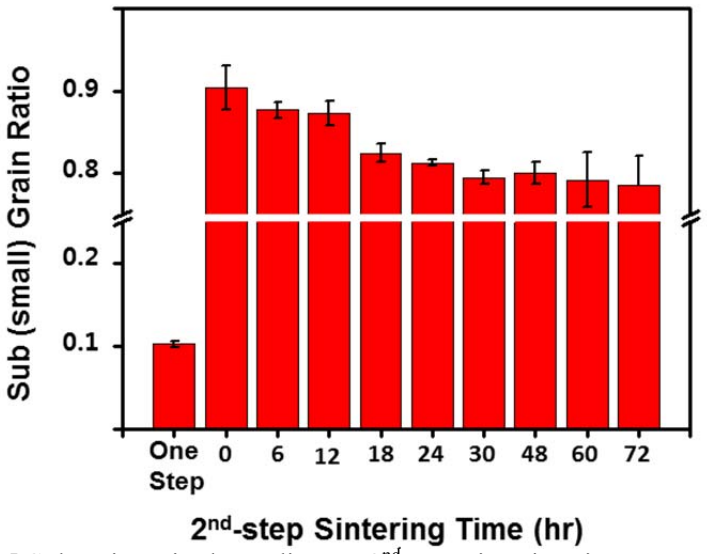

[Figure 14] Subgrain ratio depending on 2nd-step sintering time.

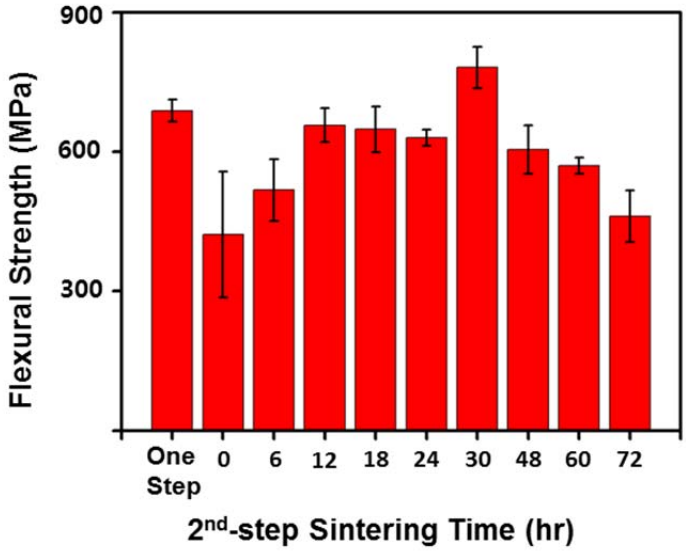

(a)

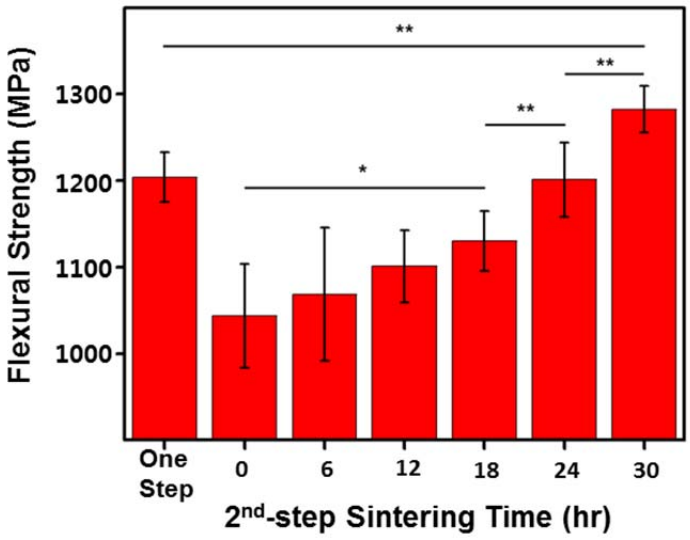

(b)

[Figure 15] Flexural strength data tested by (a) 4-point bending test and (b) biaxial bending test

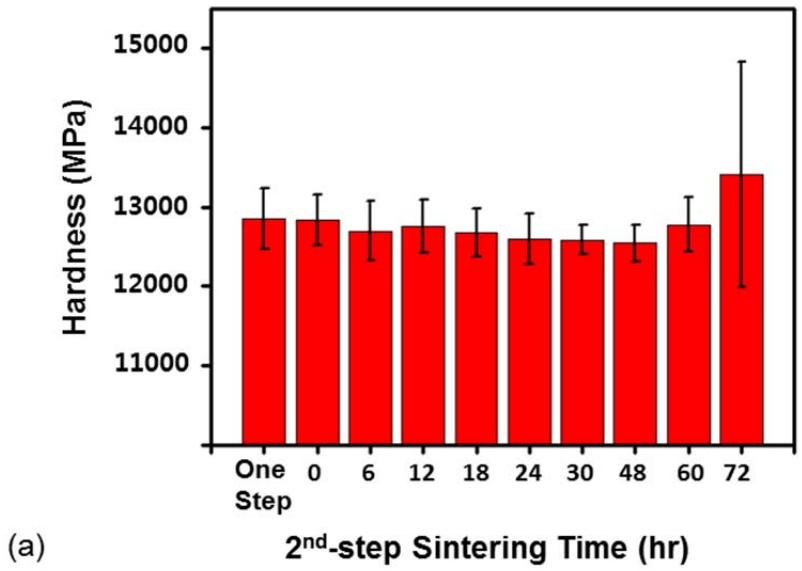

(a)

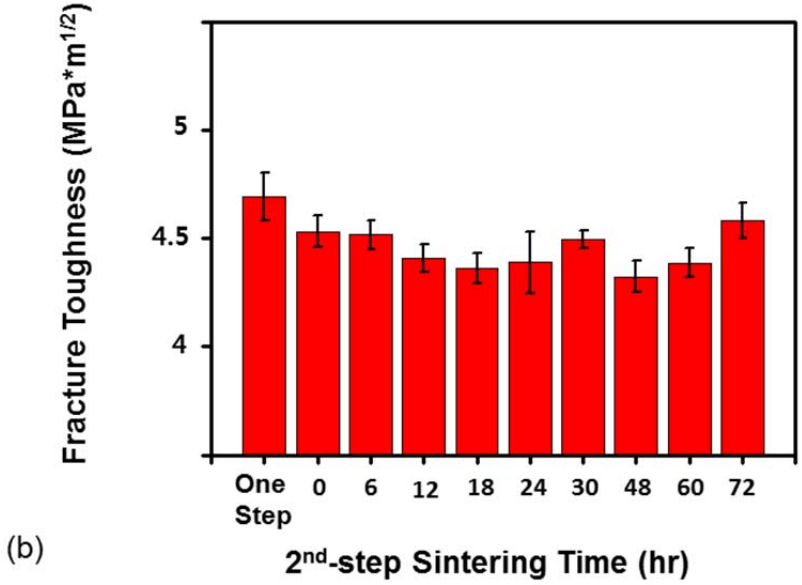

(b)

[Figure 16] (a) Hardness and (b) Fracture toughness. There is no significant difference among conditions.

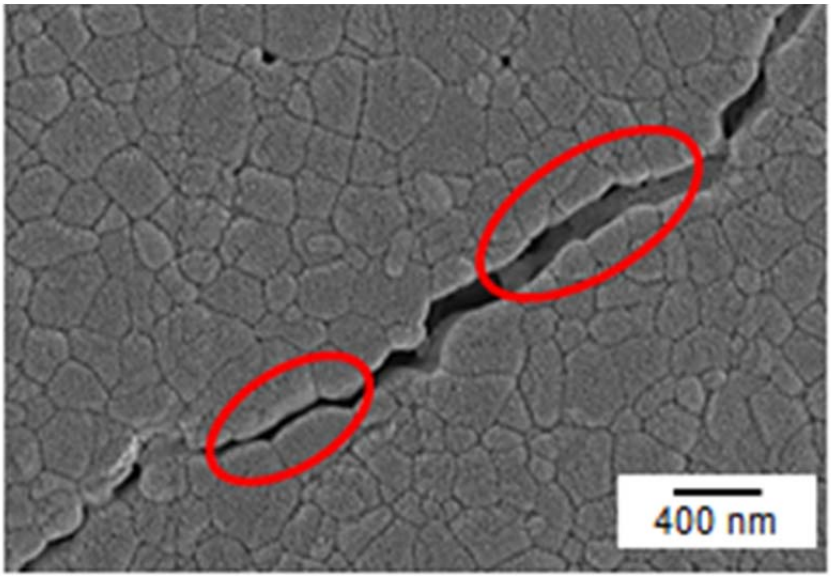

[Figure 17] The morphology of crack on the 3Y-TZP sintered by TSS surface. Crack penetrated some grains, which were marked circles.

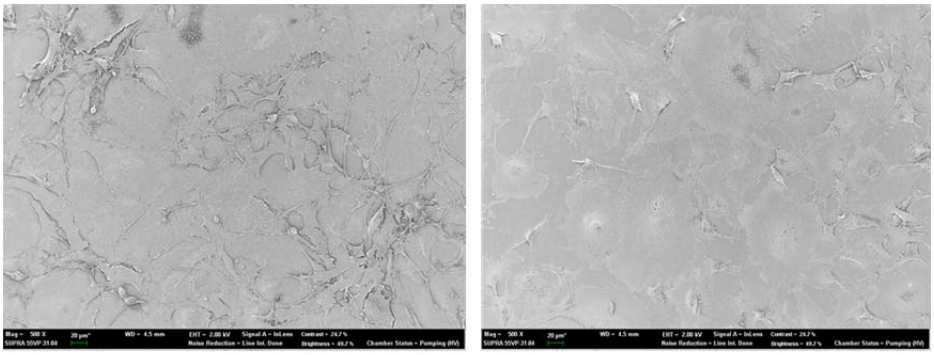

(a) (b)

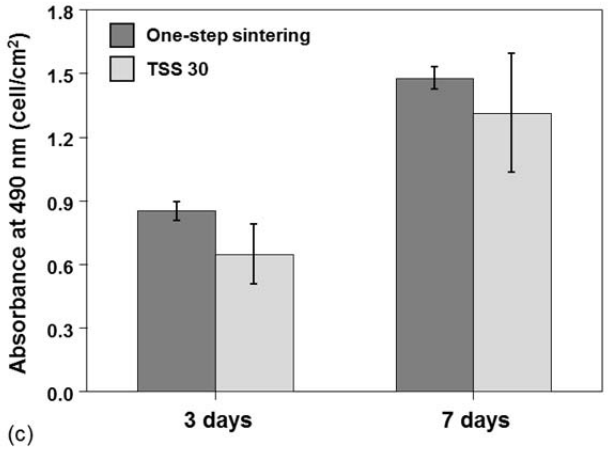

(c)

[Figure 18] Cell attachment image of (a) One-step sintered sample and (b) TSS 30. (c) Cell viability measured by an MTT assay. No statistical significance was observed between two types of 3Y-TZP for each culture time.

4. Conclusion

3Y-TZP sintered by TSS process was found to reach over 99% of the theoretical density regardless of the 2nd-step sintering time even though the relative density was observed to increase as the 2nd-step sintering time increased. Along with increasing the 2nd-step sintering time, the average grain size of 3Y-TZP was also found to increase from 153 ± 7 (0 hr sintering) to 211 ± 11 nm (72 hr sintering), which is 2 to 2.5 times as small as that of the commercial one step sintered 3Y-TZP. In particular, interesting structures, subgrains and agglomerated particles, were observed inside normal grain and some part of the surface of 3Y-TZP sintered by TSS, respectively. These structures slightly disappeared as holding time of 2nd-step became longer. We predicted the grain growth mechanism in the TSS based on the results as the relationship of the 2nd-step sintering time. In this study, because all conditions were fully dense, we confirmed that grain size and subgrain effected on the mechanical properties. Before 30 hr, grain size was increasing and subgrain ratio was decreasing, which made flexural strength increased. After 30 hr, subgrain ratio valued constant despite of the increasing grain size, which induced decreasing of the flexural strength. Flexural strength of 3Y-TZP sintered by TSS process increased up to 781 ± 45 MPa at 2nd-step sintering time, 30 hr, then considerably decreased as the 2nd-step sintering time exceeded 30 hr. Therefore, the effects of subgrain and grain size were the complete correlation, inverse relation with flexural strength. This subgrain

structure showed relation with crack propagation. 3Y-TZP sintered by TSS had cracks that penetrated inside the grain, which had subgrain, more frequently. This is the main effect on flexural strength of subgrain. However, it was believed that there exist any other factors that effected on strength besides the subgrain effect. There was not any significant difference in hardness and fracture toughness. The biological properties of 3Y-TZP also had no significant difference depending on the grain size, indicating that 3Y-TZP sintered by TSS still had very good biocompatibility without any toxicity.

5. Reference

[1] Ducheyne P, Qiu Q. Bioactive ceramics: the effect of surface reactivity on bone formation and bone cell function. Biomaterials. 1999;20:2287-303.

[2] Damien CJ, Parsons JR. Bone graft and bone graft substitutes: a review of current technology and applications. Journal of applied biomaterials : an official journal of the Society for Biomaterials. 1991;2:187-208.

[3] Glowacki J, Mulliken JB. Demineralized bone implants. Clinics in plastic surgery. 1985;12:233-41.

[4] Ginebra M-P, Canal C, Espanol M, Pastorino D, Montufar EB. Calcium phosphate cements as drug delivery materials. Advanced Drug Delivery Reviews. 2012;64:1090-110.

[5] Garcia R, Doremus RH. Electron microscopy of the bone-hydroxylapatite interface from a human dental implant. J Mater Sci: Mater Med. 1992;3:154-6.

[6] Doremus RH. Bioceramics. J Mater Sci. 1992;27:285-97.

[7] Puleo DA, Holleran LA, Doremus RH, Bizios R. Osteoblast responses to orthopedic implant materials in vitro. Journal of biomedical materials research. 1991;25:711-23.

[8] Webster TJ, Ergun C, Doremus RH, Bizios R. Hydroxylapatite with substituted magnesium, zinc, cadmium, and yttrium. Ⅱ. Mechanisms of osteoblast adhesion. Journal of biomedical materials research. 2002;59:312-7.

[9] Lee I-S, Whang C-N, Kim H-E, Park J-C, Song JH, Kim S-R. Various Ca/P ratios of thin calcium phosphate films. Materials Science and Engineering: C. 2002;22:15-20.

[10] Craig RG, LeGeros RZ. Early events associated with periodontal connective tissue attachment formation on titanium and hydroxyapatite surfaces. Journal of biomedical materials research. 1999;47:585-94.

[11] Sergo V, Sbaizero O, Clarke DR. Mechanical and chemical consequences of the residual stresses in plasma sprayed hydroxyapatite

coatings. Biomaterials. 1997;18:477-82.
[12] Choi J-M, Kong Y-M, Kim S, Kim H-E, Hwang CS, Lee I-S. Formation and characterization of hydroxyapatite coating layer on Ti-based metal implant by electron-beam deposition. Journal of Materials Research. 1999;14:2980-5.
[13] Yang Z, Yuan H, Tong W, Zou P, Chen W, Zhang X. Osteogenesis in extraskeletally implanted porous calcium phosphate ceramics: variability among different kinds of animals. Biomaterials. 1996;17:2131-7.
[14] Kurashina K, Kurita H, Wu Q, Ohtsuka A, Kobayashi H. Ectopic osteogenesis with biphasic ceramics of hydroxyapatite and tricalcium phosphate in rabbits. Biomaterials. 2002;23:407-12.
[15] Harada Y. [Experimental studies of healing process on compound blocks of hydroxyapatite (HAP) particles and tricalcium phosphate (TCP) powder implantation in rabbit mandible--comparison of HAP/TCP ratios and plastic methods]. Shika gakuho Dental science reports. 1989;89:263-97.
[16] Monma H. TRICALCIUM PHOSPHATE CERAMICS COMPLEXED WITH HYDROXYAPATITE. Yogyo Kyokai Shi/Journal of the Ceramic Society of Japan. 1987;95:814-8.
[17] Alam I, Asahina I, Ohmamiuda K, Enomoto S. Comparative study of biphasic calcium phosphate ceramics impregnated with rhBMP-2 as bone substitutes. Journal of biomedical materials research. 2001;54:129-38.
[18] Piconi C, Maccauro G. Zirconia as a ceramic biomaterial. Biomaterials. 1999;20:1-25.
[19] Becher PF, Swain MV. Grain-Size-Dependent Transformation Behavior in Polycrystalline Tetragonal Zirconia. Journal of the American Ceramic Society. 1992;75:493-502.
[20] Hannink RHJ, Kelly PM, Muddle BC. Transformation Toughening in Zirconia-Containing Ceramics. Journal of the American Ceramic Society. 2000;83:461-87.
[21] Chevalier J, Gremillard L, Virkar AV, Clarke DR. The Tetragonal-Monoclinic Transformation in Zirconia: Lessons Learned and Future Trends.

Journal of the American Ceramic Society. 2009;92:1901-20.
[22] Li Y, Kim HE, Koh YH. Improving the surface hardness of zirconia toughened alumina (ZTA) composites by surface treatment with a boehmite sol. Ceramics International. 2012;38:2889-92.
[23] Theunissen GSAM, Bouma JS, Winnubst AJA, Burggraaf AJ. Mechanical properties of ultra-fine grained zirconia ceramics. J Mater Sci. 1992;27:4429-38.
[24] Guazzato M, Albakry M, Ringer SP, Swain MV. Strength, fracture toughness and microstructure of a selection of all-ceramic materials. Part I. Pressable and alumina glass-infiltrated ceramics. Dental materials : official publication of the Academy of Dental Materials. 2004;20:441-8.
[25] Guazzato M, Albakry M, Ringer SP, Swain MV. Strength, fracture toughness and microstructure of a selection of all-ceramic materials. Part II. Zirconia-based dental ceramics. Dental materials : official publication of the Academy of Dental Materials. 2004;20:449-56.
[26] Matsui K, Yoshida H, Ikuhara Y. Grain-boundary structure and microstructure development mechanism in 2-8 mol% yttria-stabilized zirconia polycrystals. Acta Materialia. 2008;56:1315-25.
[27] Chevalier J, Deville S, Münch E, Jullian R, Lair F. Critical effect of cubic phase on aging in 3 mol% yttria-stabilized zirconia ceramics for hip replacement prosthesis. Biomaterials. 2004;25:5539-45.
[28] Bravo-Leon A, Morikawa Y, Kawahara M, Mayo MJ. Fracture toughness of nanocrystalline tetragonal zirconia with low yttria content. Acta Materialia. 2002;50:4555-62.
[29] German RM. Introduction to Sintering. Sintering Theory and Practice: JOHN WILEY & SONS, INC.; 1996. p. 1-20.
[30] KANG S-JL. Sintering Processes. Sintering-Densification, Grain Growth & Microstructure: ELSEVIER; 2005. p. 3-8.
[31] Mazaheri M, Simchi A, Golestani-Fard F. Densification and grain growth of nanocrystalline 3Y-TZP during two-step sintering. Journal of the European Ceramic Society. 2008;28:2933-9.

[32] Chen IW, Wang XH. Sintering dense nanocrystalline ceramics without final-stage grain growth. Nature. 2000;404:168-71.
[33] Mazaheri M, Zahedi AM, Sadrnezhaad SK. Two-Step Sintering of Nanocrystalline ZnO Compacts: Effect of Temperature on Densification and Grain Growth. Journal of the American Ceramic Society. 2008;91:56-63.
[34] Wang XH, Deng XY, Bai H-L, Zhou H, Qu W-G, Li LT, et al. Two-Step Sintering of Ceramics with Constant Grain-Size, II: BaTiO3 and Ni–Cu–Zn Ferrite. Journal of the American Ceramic Society. 2006;89:438-43.
[35] Bodišová K, Šajgalík P, Galusek D, Švančárek P. Two-Stage Sintering of Alumina with Submicrometer Grain Size. Journal of the American Ceramic Society. 2007;90:330-2.
[36] Loureno MA, Cunto GG, Figueiredo FM, Frade JR. Model of two-step sintering conditions for yttria-substituted zirconia powders. Materials Chemistry and Physics. 2011;126:262-71.
[37] Yu PC, Li QF, Fuh JYH, Li T, Lu L. Two-stage sintering of nano-sized yttria stabilized zirconia process by powder injection moulding. Journal of Materials Processing Technology. 2007;192-193:312-8.
[38] Reddy KM, Mukhopadhyay A, Basu B. Microstructure-mechanical-tribological property correlation of multistage spark plasma sintered tetragonal ZrO2. Journal of the European Ceramic Society. 2010;30:3363-75.
[39] Maca K, Pouchly V, Shen Z. Two-step sintering and spark plasma sintering of Al2O 3, ZrO2 and SrTiO3 ceramics. Integrated Ferroelectrics. 2008;99:114-24.
[40] Maca K, Pouchly V, Zalud P. Two-Step Sintering of oxide ceramics with various crystal structures. Journal of the European Ceramic Society. 2010;30:583-9.
[41] Suárez G, Sakka Y, Suzuki TS, Uchikoshi T, Zhu X, Aglietti EF. Effect of starting powders on the sintering of nanostructured. Science and Technology of Advanced Materials. 2009;10.
[42] Kumar BVM, Kim W-S, Hong S-H, Bae H-T, Lim D-S. Effect of grain size on wear behavior in Y-TZP ceramics. Materials Science and Engineering: A.

2010;527:474-9.
[43] Tsubakino H, Matsuura N. Relationship between transformation temperature and time-temperature-transformation curves of tetragonal-to-monoclinic martensitic transformation in zirconia-yttria system. Journal of the American Ceramic Society. 2002;85:2102-6.
[44] Theunissen GSAM, Winnubst AJA, Burggraaf AJ. Sintering kinetics and microstructure development of nanoscale Y-TZP ceramics. Journal of the European Ceramic Society. 1993;11:315-24.
[45] Mendelson MI. Average Grain Size in Polycrystalline Ceramics. Journal of the American Ceramic Society. 1969;52:443-6.
[46] Niihara K. A fracture mechanics analysis of indentation-induced Palmqvist crack in ceramics. J Mater Sci Lett. 1983;2:221-3.
[47] Trunec M. Effect of grain size on mechanical properties of 3Y-TZP ceramics. Ceramics - Silikaty. 2008;52:165-71.
[48] Rios PR, Siciliano Jr F, Sandim HRZ, Plaut RL, Padilha AF. Nucleation and growth during recrystallization. Materials Research. 2005;8:225-38.

초록

생체세라믹은 하중을 지지하지 않는 임플란트로는 물론 하중을 지지하는 임플란트로도 널리 사용되고 있다. 이들 재료는 생활성 세라믹스와 생불활성 세라믹스로 나눌 수 있다. 하이드록시아파타이트, 삼인산칼슘 등의 생활성 세라믹스는 주사가 가능하고 낮은 온도에서 가공이 가능하며 조직과 뼈의 재생을 촉진시킨다는 장점을 가지고 있다. 반면, 산화알루미늄과 산화지르코늄 등의 생불활성 세라믹스는 재생 촉진 등의 장점은 없지만 좋은 생체적합성과 매우 뛰어난 기계적 성질을 지니고 있다. 그 중, 3Y-TZP는 다른 생불활성 세라믹스에 비해 뛰어난 기계적 특성들을 가진다.

임플란트에 사용되는 세라믹 재료의 기계적 성질들을 더 향상시키기 위해 많은 연구자들이 노력을 해왔다. 이들은 특히 세라믹의 결정립 크기를 조절하는 연구에 초점을 맞추어 진행해왔고, 마침내 2000년도에 Chen과 Wang이 낮은 온도에서 매우 긴 시간 동안 세라믹 재료를 소결하는 2단계 소결(TSS)을 고안하였다. 그들은 약 300도 정도 낮은 소결 온도를 갖는 2단계 소결을 통해 완전히 치밀하면서도 기존보다 훨씬 작은 결정립 크기의 재료를 얻을 수 있었다. 이 공정이 발표된 후, 2단계 소결을 거친 3Y-TZP에 대한 연구가 많이 진행되었다. 하지만, 그 중에서 3Y-TZP의 기계적 성질에

대해 언급한 연구는 찾아볼 수 없었다.

본 연구에서는, 2단계 공정에서 2번째 소결 시간을 다양하게 하여 3Y-TZP의 기계적 성질들을 측정하고 미세구조를 관찰하였다. 완전히 치밀한 3Y-TZP를 얻기 위해 1번째 소결에서 1450도에서 15분 동안 소결하였고, 이후 2번째 소결에서는 1150도에서 0, 6, 12, 18, 24, 30, 48, 60, 72시간 동안 소결하였다. 소결된 3Y-TZP들은 상대밀도, 결정립 크기, 미세구조, 기계적 성질들(강도, 경도, 파괴 인성)과 세포실험을 통해 평가하였다. 2단계 소결을 거친 모든 3Y-TZP는 2번째 소결 시간이 증가함에 따라 상대밀도가 증가하는 것을 확인했다. 또한, 모든 조건에서 이론밀도의 99% 이상의 밀도로 완전히 치밀한 것을 알 수 있었다. 평균적인 결정립 크기도 153 ± 7 nm (0 시간)에서 211 ± 11 nm (72 시간)으로 2번째 소결 시간에 비례하는 것을 확인했다. 이는 기존의 1단계 소결을 거친 3Y-TZP에 비해 약 2~2.5배 정도 작은 것이다. 특히, 흥미로운 점은 부결정립과 입자들이 뭉쳐있는 미세구조들이 2단계 소결을 거친 재료의 결정립의 내부와 표면에서 관찰되었다는 것이다. 우리는 2번째 소결 시간과 미세구조의 모양, 결정립 크기에 따른 결과들을 바탕으로 2단계 소결에서의 결정립 성장과정을 예측할 수 있었다. 또한, 모든 조건이 완전히 치밀하기 때문에, 결정립의 크기와 부결

정립 등의 미세구조가 기계적 성질에 미치는 영향을 확인할 수 있었다. 강도는 앞의 결과들과 다른 경향을 보였다. 2번째 소결 시간이 30 시간인 시점(이 때 강도는 781 ± 45 MPa)을 기준으로 그 전에는 강도와 소결 시간이 비례하였지만, 그 이후에는 반비례 관계임을 보였다. 따라서, 부결정립과 결정립 크기의 효과 모두 강도와 반비례의 관계에 있다는 것을 확인하였다. 미세구조 관찰을 통해서 부결정립 구조가 강도에 미치는 영향은 균열의 성장과 관련이 있다는 것을 알 수 있었다. 2단계 소결을 거친 3Y-TZP는 부결정립을 가지는 결정립 내부를 관통하는 균열을 가지는 빈도가 높았고, 이것이 부결정립이 강도에 부정적인 영향을 미치는 이유라고 판단하였다. 하지만, 실험 결과들에 비추어 볼 때, 결정립의 크기와 부결정립의 효과 외에 강도에 영향을 주는 다른 요인들도 존재할 것이라 추정했다. 강도와 파괴 인성의 경우 각 조건에 따라 큰 차이가 없었다. 또한, 3Y-TZP의 생체 특성도 결정립의 크기와 상관없이 독성이 없고 여전히 좋은 생체적합성을 지님을 알 수 있었다.

주요어: 3Y-TZP, 2단계 소결, 2번째 소결 시간, 기계적 성질, 결정립 크기, 부결정립.

학번: 2012-23145